Sensing in Electroanalysis

Vol. 7 (K. Kalcher, R. Metelka, I. Švancara, K. Vytřas; Eds.), pp. 211–234.

ISBN 978-80-7395-563-2 (printed); 978-80-7395-564-9 (on-line)

All-Solid Nafion®-Based Amperometric Sensors for Monitoring Gaseous Oxygen

K. Wallgren[1], **I. Mintsouli**[2], **S. Papadimitriou**[2], **A. Papaderakis**[2], and **S. Sotiropoulos**[2]*

[1] *School of Chemical, Environmental and Mining Engineering, University of Nottingham, Nottingham, NG7 2RD, UK*

[2] *Laboratory of Physical Chemistry, Department of Chemistry, Aristotle University of Thessaloniki (AUTH), Thessaloniki 54124, Greece*

Abstract: Oxygen reduction has been studied at three different designs of Au/Nafion®-based all-solid amperometric sensors. These consisted of a planar-type sensor (PTS) with all electrodes sputtered on the same face of the Nafion® membrane, a capillary planar type sensor (CPTS) with the introduction of a cover bearing a capillary, and a sandwich-type sensor (STS) with the working and counter electrode layers deposited on different sides of the polymer electrolyte membrane. The response of all sensors depended heavily on humidity and the degree of Nafion® hydration but, unlike the CPTS and STS configurations, no signs of a limiting current were recorded during voltammetric experiments at an open PTS device, indicating the absence of a significant diffusion barrier in that case. All three simple and inexpensive polymer-based sensors compared well with a commercial fuel cell-type sensor, regarding their response to gaseous oxygen concentration changes.

Keywords: Oxygen sensors; Amperometric sensor; Polymer electrolyte; Nafion®.

---

*) Author to whom correspondence should be addressed. E-mail: eczss@chem.auth.gr

Introduction

Commercially available amperometric gas sensors usually involve a metallised gas-permeable porous material in contact with an internal electrolyte (liquid type sensors, LTS; [1-2]). This

type of design has been found to lead to slow response times due to the gas diffusion through the porous medium and the liquid film, as well as because of limited lifetime caused by occasional drying out of the liquid film. The use of a solid ionic conductor as an electrode substrate allows the active electrode material to be directly exposed to the gas sample, improving the response time and sensitivity of the device [3-5].

All-solid electrochemical gas sensors are not prone to drying-out problems but are often dependant on humidity (in which case a correction should be made). There are two main arrangements for such sensors. In the most common one, the solid ionic conductor (e.g. Nafion® [6,7], antimonic acid [8,9] or Zr phosphates and phosphonates [10,11]) is sandwiched between the working and counter electrodes (sandwich type sensors; STS). Since the gas has to diffuse through the metal layer to reach the working electrode-electrolyte interface, a well-characterised mass transfer barrier exists and the current vs. potential curves can in some cases (e.g. for oxygen reduction at Pt, Au and Ag) have an S-shaped form with a limiting current plateau.

In an alternative design for all-solid amperometric gas sensors, all the electrodes are deposited or attached on the same face of the ionic conductor, separated by an uncovered strip of electrolyte, and in direct contact with the gas sample (planar type sensors, PTS; [12-14]). In the latter case, it was suggested that due to the non-porous nature of the electrodes and the arrangement used in that design, the gas is preferably reacting at locations close to the line formed between the working electrode metal layer, the solid electrolyte and the gas sample. Potential advantages of this design include faster response times and higher sensitivities per useful electrode area. The mass-transport rates of the gas to the sensing electrode are higher since no significant membrane or liquid film barrier is expected at the locus of the electrode reaction. Furthermore, smaller quantities of precious metal catalyst could be used for the working electrode as the reaction is occurring at the edge of the deposit and hence a thin line of catalyst should suffice. Finally, the labour-intensive stacking steps required for the fabrication of sandwich-type designs could be avoided. Regarding the shape of the current-potential curves at the PTS arrangement, no signs of a mass transport limiting current plateau were observed. This can be anticipated for a slow electrode reaction such as that of oxygen reduction on Au, and indicates that the reaction is under kinetic or at least mixed control at the high rates of diffusion in the absence of a well-defined barrier. However, the presence of a limiting, potential independent current, is often a requirement for stable amperometric sensor operation, that should tolerate moderate applied potential fluctuations; this barrier can be introduced by the presence of a porous membrane or a capillary.

Based on the above, the various types of diffusion control encountered in amperometric gas sensor configurations can be summarised as follows:

(i) Analyte gas diffusion through a condenced phase diffusion barrier:
- Liquid phase diffusion through a liquid electrolyte film (in LTS devices)
- Solid state diffusion through a non-porous membrane (in STS devices)

(ii) Analyte gas diffusion from the gas phase (in PTS devices) :
- Gas phase diffusion through a macroporous membrane or capillary
- Gas phase diffusion through a micro-porous membrane (Knudsen diffusion)

Each of them has differing responses to temperature and pressure that can have advantages to particular applications [15].

In this paper, we present results aimed at the comparison of three different designs of a Au/Nafion®-based all-solid amperometric sensor: (**a**) a "sandwich-type" sensor (STS) arrangement with the working electrode (WE) and counter electrode (CE) layers deposited on different sides of the Nafion® membrane; (**b**) a planar-type sensor (PTS) with all electrodes on the same face of the Nafion® membrane and (**c**) a capillary/planar-type sensor (CPTS), with the introduction of a lid bearing a capillary opening over the PTS device. The behaviour of the sensors to oxygen concentration and humidity changes is studied and the shape and magnitude of current vs. potential curves is also discussed.

Experimental

Sensor Fabrication

Nafion® membranes (Nafion® 117 protonised form, 180 μm thick, Aldrich) were washed thoroughly with distilled water before stored in distilled water. A piece of membrane, of typical dimensions of 40x40 mm, was cut when required and dried using lint-free tissue paper prior to use.

The metal layers of the working and counter electrodes (WE and CE) were vacuum-deposited onto the polymer substrates using varying numbers of deposition cycles with a PS3 E500C Series 3 Polaron sputter-coater. A coating step of 1s gave a ca. 1.5 nm thick Au layer and the final Au layer thickness of the sensors was 360 nm. A 0.5 mm thick stainless steel sheet with machined openings was used as a mask during vacuum metal deposition of the electrode layers. A piece of the membrane with the mask onto one of its faces (for planar, PTS and CPTS devices) was attached tightly to a 40 mm

square stainless steel slide before being placed in the sputtering chamber. For sandwich, STS, devices the procedure with the appropriate mask was repeated for the opposite face, too. Electrical contacts between commercial insulated wires and the metal deposits were made either with the help of Ag-loaded epoxy resin (RS) (with Araldite epoxy resin (RS) providing insulation and mechanical strength to the contact) or with crocodile clips in contact with small pieces of aluminum foil pressed onto the electrode surfaces. In the last case, the aluminum foil was acting as a current collector. For the three-electrode experiments presented in this study, a strip of screen-printed Ag/AgCl electrode was placed next to the working electrode layer (for PTS and CPTS co-planar electrode devices) or on the opposite face of the membrane (for sandwich, STS, arrangements) and pressed onto the membrane with a crocodile clip.

A top-view drawing of the planar (PTS) device used is given in Fig. 1(A). The lengths of the working electrode (WE) and the counter electrode (CE) parallel to each other are 5 mm and 30 mm respectively and these were separated by a Nafion® path 5 mm wide. The electrode arrangement for the sandwich-type, STS, device is given in Figure 1(B) for both front and back faces of the membrane.

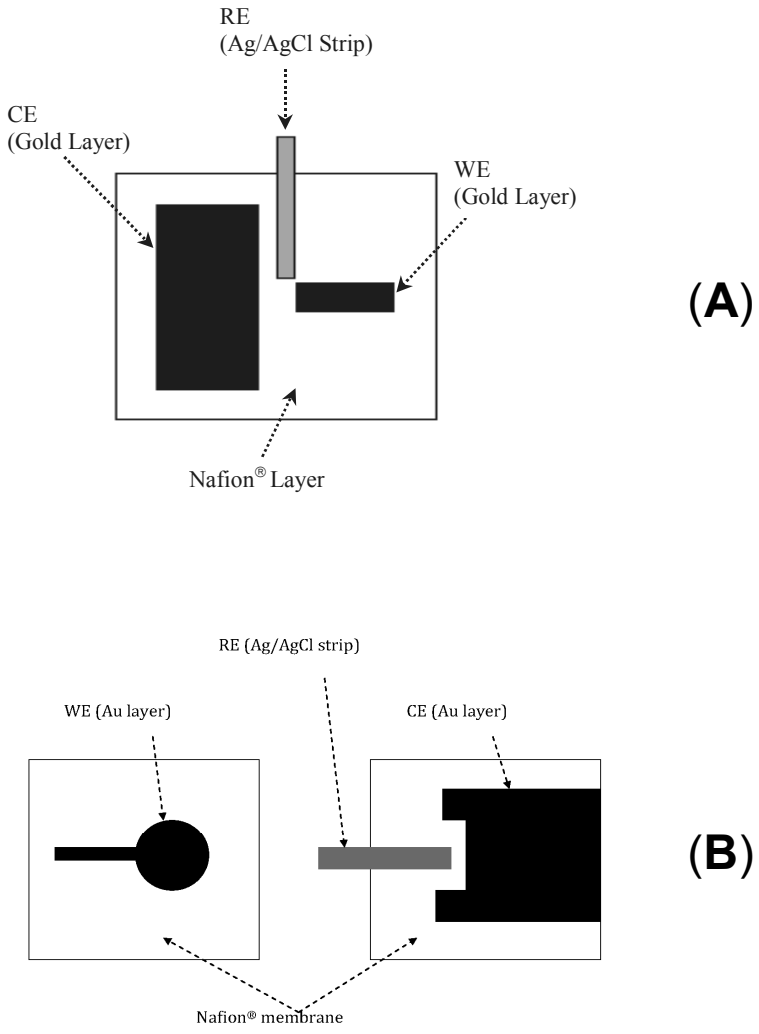

Fig. 1:
Schematic diagrams of (**A**) *a planar-type sensor, PTS, with a co-planar arrangement of all electrodes and* (**B**) *the two sides of a sandwich-type sensor, STS, with the counter, CE and reference, RE, electrodes on the opposite face of the membrane from that of the working electrode, WE..*

For the capillary-planar-type sensor, CPTS, the assembly of Figure 1(A) was encased in a cell made of a PVC body and a lid made of Nylon®, with a 1.5mm hole acting as a capillary. Strips of platinum were used as current collectors. The metal/polymer composite was inserted in the cell bottom plate and held tightly onto it with the lid.

Electrochemical Equipment

For the three-electrode experiments presented in this paper two different potentiostats were used. For preliminary cyclic voltammetry and oxygen concentration step experiments, a Radiometer Voltamaster 21® potentiostat, interfaced to a 486 PC by a Duo 18 A/D converter, was used. The majority of experiments were performed with an Autolab PGSTAT30 potentiostat controlled by GPES software version 4.5 (for Windows 95).

Cell and Gas Mixtures

Experiments were carried out in a 500 ml glass cell, equipped with a wall-jacket and a gas inlet and outlet. The temperature of the cell was controlled by circulating water in the jacket from a thermostatic bath (25°C). The composition of the atmosphere in the cell was maintained by gas feeds (of either laboratory compressed air-21% oxygen or 4%, 8%, 12%, 16% oxygen/nitrogen mixtures and pure nitrogen, all from Air Products Ltd, 99.998%). The gas mixtures were first passed through two Dreschler-type flasks at a ca. 100 ml min^{-1} flow rate. To achieve 100% relative humidity distilled water was used in both flasks while for other humidity levels appropriate KOH or LiCl solutions were used [16] (humidity was confirmed with a TESTO6400 RS hygrometer).

Results and Discussion

Planar Type Sensors (PTS): Voltammetry

Fig. 2 (overleaf) shows a cyclic voltammogram recorded at 50 mV/s at a three-electrode Au (vs. Ag/AgCl) / Nafion® / Au assembly with all electrodes on the same face of the membrane in a water-saturated air stream.

A well-defined voltammogram, typical of aqueous Au-electrochemistry (see for example [17]) was recorded. This includes the oxide formation plateau in the +0.85 to +1.25 V vs. Ag/AgCl range, and its stripping-reduction peak at –0.45 V vs. Ag/AgCl. A crude estimate of the area below this cathodic peak gives an approximate charge of 606 μC.

Since the charge corresponding to the formation/stripping of a Au monolayer on a smooth Au electrode is known from the literature to be 420 μC/cm^2 [4, 18, 19], the true active electrode area of the working electrode is estimated to be as high as 1.4 cm^2.

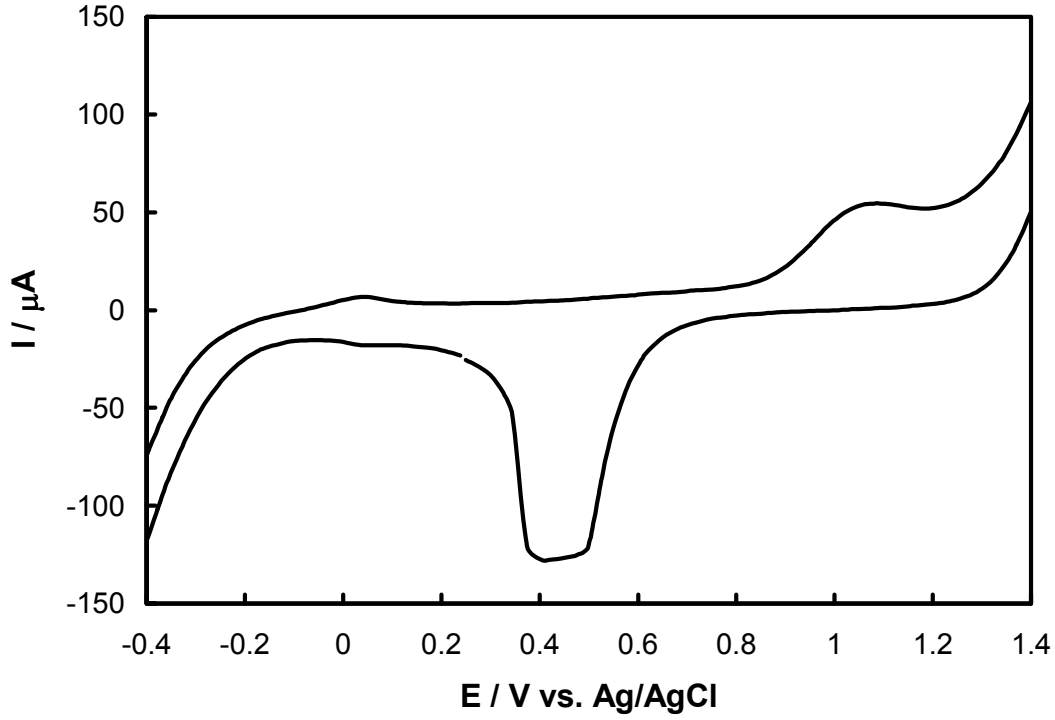

Fig. 2: *Voltammogram recorded at 50 mV/s in a water-saturated air stream at a three-electrode Au (vs. Ag/AgCl)/Nafion®/Au PTS planar device.*

Using the roughness factor of similar Au-deposits on Nafion® (reported to be anywhere in the 10-100 range [18, 19]), and the length of the working electrode edge parallel to the CE layer (0.5 cm), the effective depth of the electrode layer in the direction away from the CE layer that undergoes Au surface reactions can be estimated. The uneven current distribution encountered at this type of planar electrode arrangement (i.e. the electric field focusing between the two opposing edges of the coplanar WE and CE electrode layers) results in the current passing through an estimated apparent working electrode area of 0.28 cm wide x 0.5 cm long (0.14 cm^2) or 0.028 cm wide x 0.5 cm long (0.014 cm^2), depending on whether a roughness factor of 10 or 100 is assumed. Note that the nominal planar geometric area of the entire WE layer is 1.25 cm x 0.5 cm = 0.625 cm^2 and hence, the electroactive area is only a fraction of the nominal area.

These calculations hold for the given current range (100 μA) and conductivity conditions (water-saturated polymer substrate) which determine the current and potential distribution in the planar electrode arrangement.

Fig. 3 (on bottom) presents voltammograms recorded at 5 mV/s in water-saturated air and nitrogen streams with the same device. At the moderate polarisations shown here, there is a clear exponential rise of the current in the presence of oxygen. The difference between forward and reverse scans at higher potentials could be due to partial proton depletion of the electrolyte as oxygen reduction proceeds ($O_2 + 2H^+ + 2e^- \rightarrow H_2O_2$ and $H_2O_2 + 2H^+ + 2e^- \rightarrow 2H_2O$, on Au). The current keeps rising exponentially up to moderate polarisations, with no signs of a limiting current even at extreme negative potentials up to –1.0 V (not shown here). Note that in aqueous acid solutions, oxygen reduction on Au electrodes does show a limiting current (see for example [20]). This indicates that oxygen reduction on Au at the PTS device is never under mass transfer control (at least in the 4-25 % concentration range studied in this set of experiments).

Such behaviour would be expected for a fuel-cell type porous electrode but in the case of a uniform Au layer of no macroporosity (as confirmed by SEM micrographs-not shown) and limited gas permeability, it could only be possible if oxygen reduction occurs primarily at the metal/Nafion®/gas line formed at the edge of the Au deposit or/and through the permeable 175 μm thick Nafion® membrane, i.e. in the absence of a significant mass transfer barrier (compared to the very slow kinetics of oxygen reduction on Au).

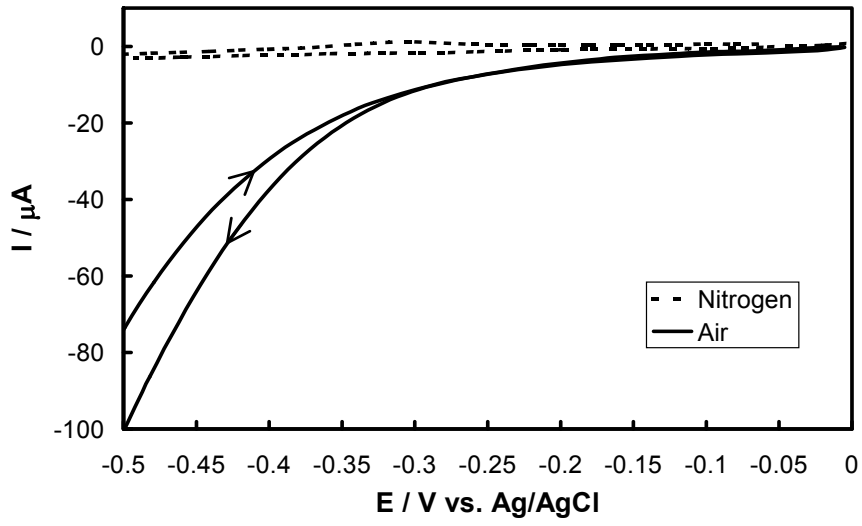

Fig. 3: *Voltammograms recorded at 5 mV/s in water saturated air and nitrogen streams at a three-electrode Au (vs. Ag/AgCl)/Nafion®/Au PTS planar device.*

The possibility of oxygen diffusing through the thin (0.35 μm thick) Au layer can also be dismissed at this stage on the following grounds. In experiments where the gas flow rate was varied in the 50-600 ml/min range, no flow dependence of the current was found even at extreme potentials where, in the presence of a thin mass transport barrier, the current should be at least under a mixed mass transport and kinetic control. Schiavon et al. [4] used Au layers on Nafion®, with the latter in contact with the electrolyte where the CE lied .

In such an arrangement oxygen had to diffuse through their 0.1 μm metal layer, and they did indeed find an increase of the signal with increasing flow rate until the former stabilised at flow rates higher than 100 ml/min. The same authors also observed a clear limiting current plateau for oxygen reduction on their devices, using alkaline internal electrolytes [4].

Planar Type Sensors (PTS): Humidity Effects

The behaviour of the Au/Nafion®/Au device was studied with respect to both Au surface electrochemistry and oxygen reduction in water-saturated samples of varied relative humidity (RH) in the 15-85 % RH range. Fig. 4 shows cyclic voltammograms at a 50 mV/s sweep rate in nitrogen samples of 36.5%, 77% and 83% RH.

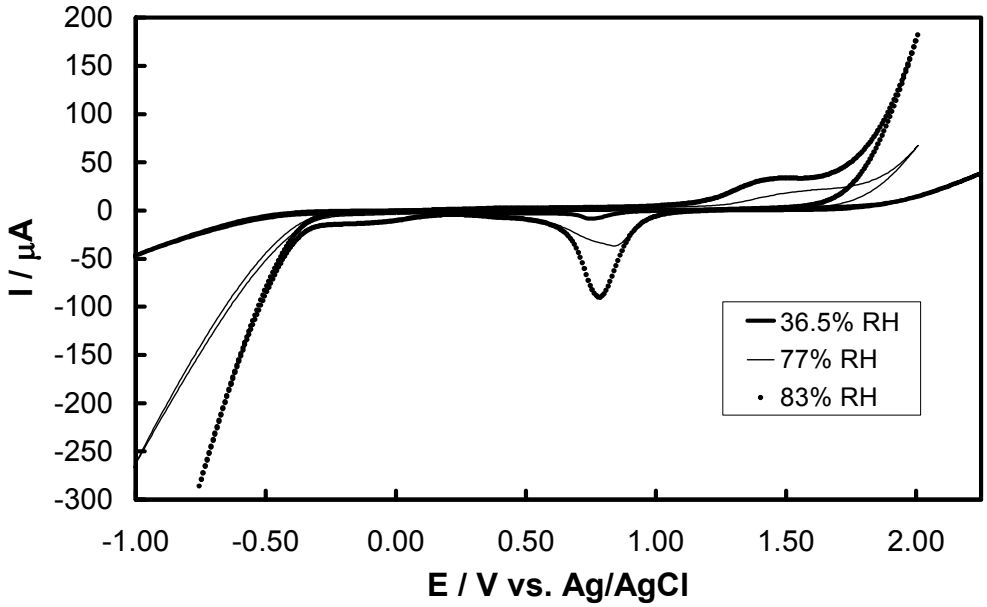

Fig. 4: *Voltammograms recorded at 50 mV/s in water saturated nitrogen streams of 36.5, 77, and 83% RH at a three-electrode Au (vs. Ag/AgCl)/Nafion/Au-planar device.*

It can be seen that it is mainly the size, and not so much the position or shape, of the oxide formation and stripping peaks that changes with humidity. Therefore, it seems that the well-known decrease in Nafion® conductivity with decreasing humidity [21-23] does not result in significant IR-distortion of the voltammetric picture. This can only be understood if there is a simultaneous inherent decrease in the currents associated with Au surface electrochemistry as the water content of the membrane decreases. Fig. 5(A) overleaf shows slow-potential-sweep (5 mV/s) voltammograms for oxygen reduction from air streams of 83.6% and 55% RH, while Fig. 5(B) depicts similar voltammograms from 36% and 23% RH streams. As seen, a similar — but much more pronounced — effect of humidity on the oxygen reduction signal is observed.

The results of a systematic study of the effect of gas relative humidity on uncompensated membrane resistance, the charge corresponding to Au oxide stripping and the oxygen reduction current at a given potential taken from the slow voltammograms, are all shown in Table I (again, see overleaf). The continuous variation of both the Au surface oxide quantity-charge and of the oxygen signal (to a different extent each) can be clearly seen. The uncompensated resistance R_u between the Au working electrode and the Ag/AgCl reference electrode was determined by the current interrupt technique (at 50-60 μA current levels). This technique is expected to give an estimate of the real ohmic losses encountered during the potentiostatic operation of the planar three-electrode devices. It was used for the IR compensation on potentiodynamic curves, which showed that at potentials where the sensors were used in the constant-potential mode (see below), the compensated and uncompensated curves nearly coincide. The high resistance values found are likely to be due to the high working electrode / reference electrode separation of (ca. 1 mm) when compared with the thickness of the Nafion® path (typically 0.1778 mm) in sandwich-type arrangements.

It should be noted however that the nearly tenfold increase in R_u for the Nafion®-based device when the %RH increases from 36 to 83.6 (from 10,800 ohm to 1,470 ohm) is in qualitative agreement with the increase of Nafion® specific conductivity from $5x10^{-3}$ Scm^{-1} (30%RH) to $3.5x10^{-2}$ Scm^{-1} (85% RH), measured by Sone et al. [22] or from $4.4x10^{-3}$ Scm^{-1} (31%RH) to $2.8x10^{-2}$ Scm^{-1} (81%RH), measured by Sumner et al [23]. As argued previously, the well-defined voltammetry of Figs. 2 and 4 indicates that the current decrease observed in both Au surface electrochemistry and oxygen reduction is unlikely to be due to the effect of humidity on conductivity alone. The number of water molecules per sulphonic group of the Nafion® polymer electrolyte is known to vary from 2 to 12 in the 20-100 %RH range and up to 14 in water-equilibrated membranes [21].

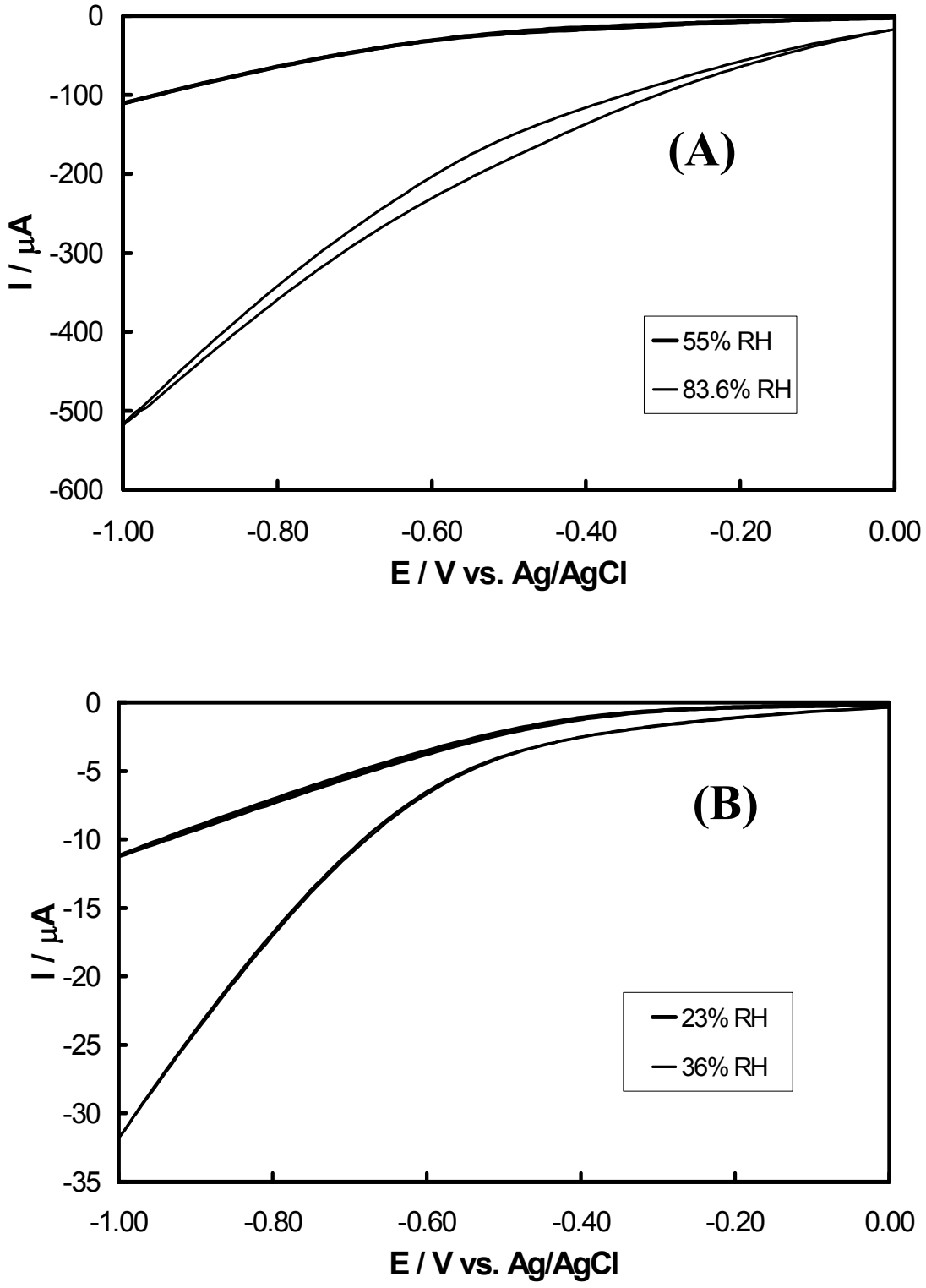

Fig. 5. *Voltammogram recorded at 5 mV/s in air streams of 55 and 83.6% RH at a three-electrode Au (vs. Ag/AgCl)/Nafion®/Au-planar device* (**A**)*. Same as (A), but for air streams of 23 and 36% RH* (**B**).

Table I: *Gold oxide reduction charge (Q), oxygen reduction signal (I) at –0.3V vs. Ag/AgCl and uncompensated resistance (R_u) in varied relative humidity (RH) conditions*

RH / %	**Q** /μC	**I** / μA	$\mathbf{R_u}$ / Ω
17.5	3.0	-0.15	70000
23	5.8	-0.66	40000
36	31.8	-1.66	10800
40.5	39	-2.60	9300
45.5	46.7	-2.70	7300
55	83.6	-10.00	4950
82.5	266.0	-84.00	1500
83.6	319.0	-86.50	1470

The ionic-aqueous regions within the polymer are expected to be the active sites for both Au oxide formation/stripping and oxygen reduction, since Au oxide formation requires water as a reactant and both Au oxide stripping and oxygen reduction require a mobile-solvated proton as a reactant. Also, the amount of water present in the polymer determines the degree of dissociation of the sulphonic acid groups, which in turn determines the proton activity and hence affects both the thermodynamics and the rate of oxygen reduction and Au oxide formation/reduction.

In an attempt to clarify whether there is the same humidity effect on both Au surface electrochemistry and oxygen reaction (e.g. a simple active site variation effect) we normalized the oxygen reduction currents with respect to the corresponding Au oxide stripping charges. Most of the values used are those given in Table I. This was done by first translating the charge values into Au electroactive surface areas (based on the 420 μC/cm^2 reported for a AuO monolayer on smooth Au [17-19]) and then converting the currents into current densities (current per electroactive surface area). Hence, the current densities reported serve as an indicator of the water content effect on two different processes: Au surface electrochemistry and oxygen reduction.

Figure 6 presents the variation of these current densities with relative humidity. It can be seen that, within the experimental uncertainties involved in calculating electroactive surface areas from repetitive cyclic voltammetry, the current density for Nafion®-based devices varies little with humidity at RH less than ca. 60%.

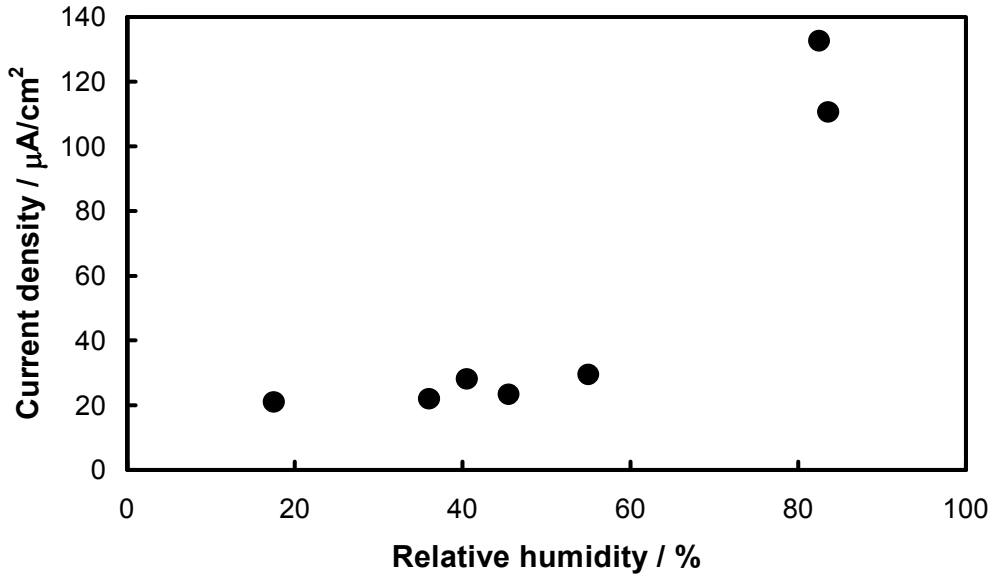

Fig. 6: *Variation of oxygen reduction current density with relative humidity of air streams for a three-electrode Au (vs. Ag/AgCl)/Nafion®/Au-planar device.*

This indicates that a mere decrease in the number of Au sites in contact with water can explain the variation of both surface electrochemistry and oxygen reduction. However at RH above ca. 70%, the increase in water content enhances significantly the reduction of oxygen. Zawodzinski et al [21] reported that at relative humidities below 75% the water in Nafion® is bound to the ions of the polymer (solvation water) whereas at higher humidities any additional water fills the polymer channels and pinholes and swells the membrane. This water has been postulated by Zecevic et al. [24] to form a very thin continuous layer between the electrode and the polymer and is believed to enhance the catalytic activity of the electrode with respect to oxygen reduction at the metal/Nafion® interface [25].

Planar Type Sensors (PTS): Oxygen Concentration Steps

Fig. 7 presents the current vs. time response of a three-electrode Au (vs. Ag/AgCl)/ /Nafion®/Au planar sensor to oxygen changes in a well humidified gas stream at constant potential of –0.1 V vs. Ag/AgCl with the response of a commercial CiTiceL® (City Technology Ltd.) shown for comparison. A smooth change of the signal with oxygen concentration was observed with indication of some saturation of the signal of interest at the higher concentration range.

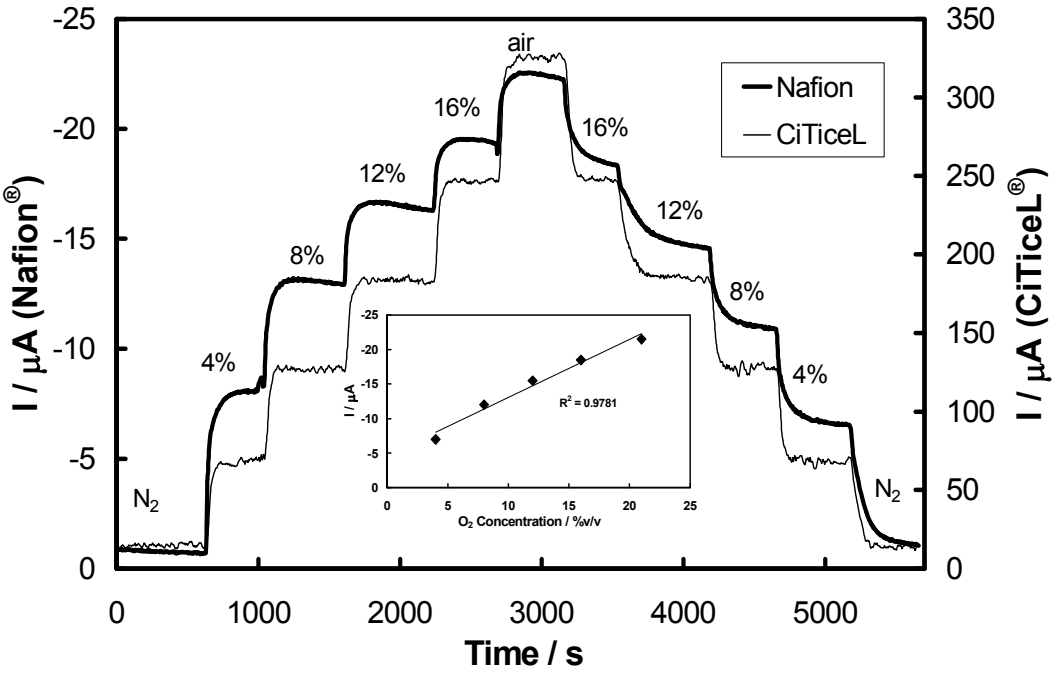

Fig. 7: *Current-time response of the Au (vs. Ag/AgCl)/Nafion®/Au PTS and CiTiceL® (City Technology Ltd) sensors to oxygen concentration steps in water saturated gas samples. The working electrode was held at –0.1 V vs. Ag/AgCl. Fig. inset: Variation of the background corrected current with oxygen concentration.*

To investigate if the response of the sensor to oxygen concentration steps is still nearly linear at humidity levels other than 100% RH (a point of high practical importance), the experiment was repeated in gas streams of lower relative humidity. Fig. 8 (overleaf) presents the current vs. time response of the same Au (vs. Ag/AgCl)/Nafion®/Au device to oxygen changes in gas streams of 50% (A) and 35% (B), at constant working electrode potentials of –0.3 V and –0.5 V vs. Ag/AgCl, respectively. The insets show the variation of the background corrected oxygen reduction current with oxygen concentration in the gas streams. Again, similar step-wise patterns to that of a well-humidified sample are observed with a smooth change of the signal. It can be seen that the slight signal saturation already at 100% RH encountered does not increase with decreasing humidity and conductivity.

Sandwich Type Sensors (STS): Voltammetry

Fig. 9 presents a cyclic voltammogram recorded at 50 mV/s in 60% RH nitrogen and air streams at a three-electrode Au (vs. Ag/AgCl)/Nafion®/Au sandwich device, where the gold layer thickness was approximately 1500 nm.

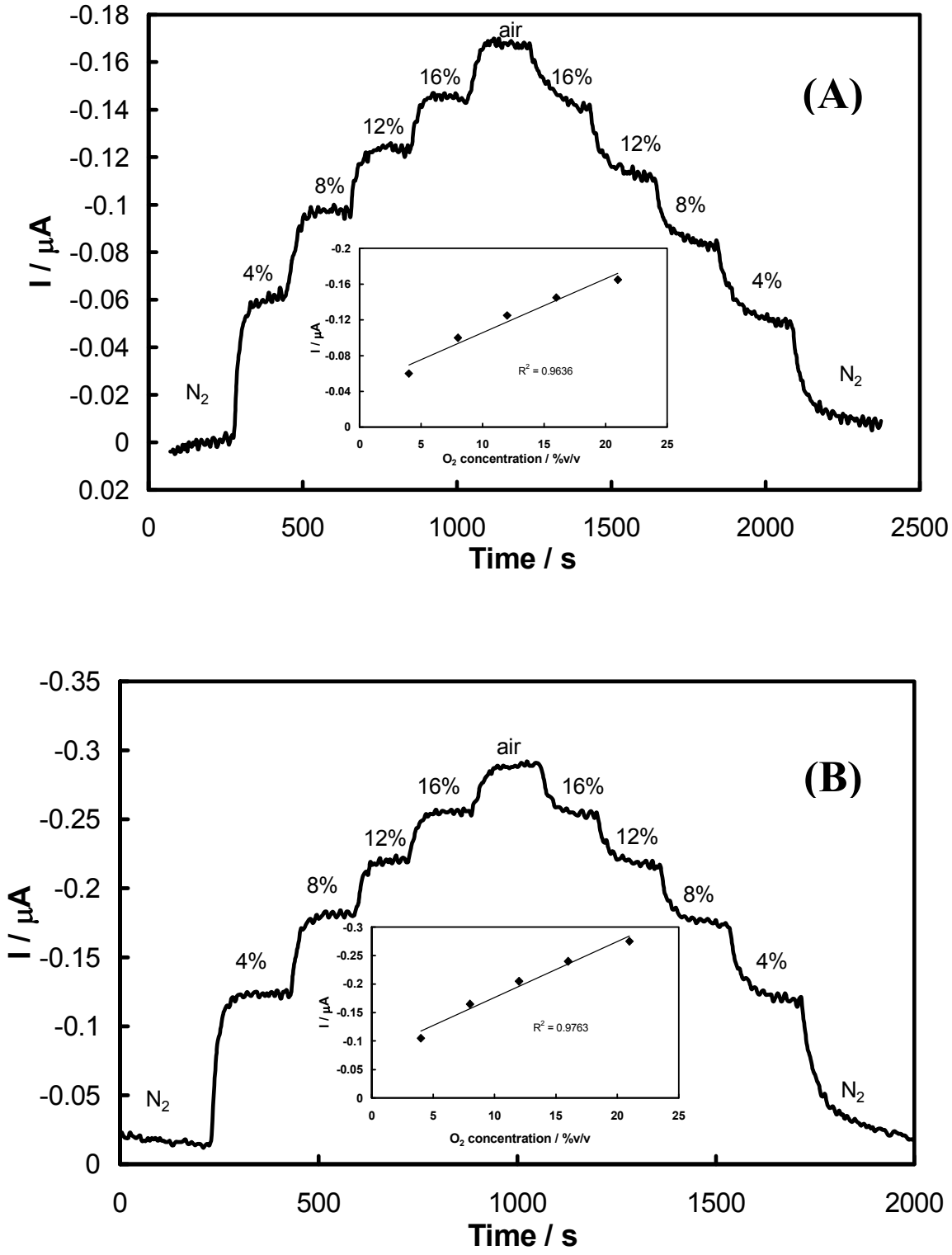

Fig. 8: *Current-time response of the Au (vs. Ag/AgCl)/Nafion®/Au sensor to oxygen concentration steps at 50% RH* (**A**) *and 35% RH* (**B**) *gas samples. The working electrode was held at -0.3 V (A) and -0.5 V (B) vs. Ag/AgCl. Inset in figure: Variation of the background corrected current with oxygen* concentration.

A sigmoidal curve is obtained in the presence of oxygen at potentials more negative than 0 V and signs of a peak or plateau are observed around –0.3 V. This suggests the existence of mass transfer limitations, in this case due to the Au layer.

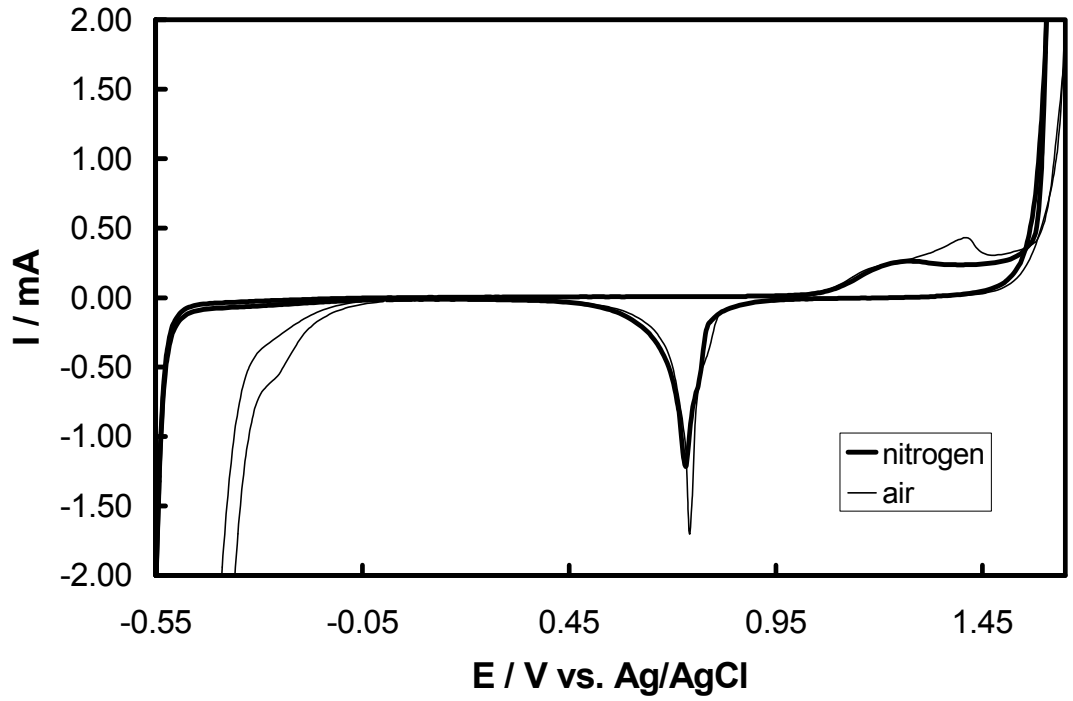

Fig.9 *Voltammograms recorded at 50 mV/s in 60% RH nitrogen (thick line curve) and air (thin line curve) streams at a three-electrode Au (vs. Ag/AgCl)/Nafion®/Au STS sandwich device with a gold layer thickness of 1500 nm.*

Fig. 10 (overleaf) presents the slow scan voltammograms (at 5 mV/s) in air and nitrogen gas streams at 60% RH. An ill-defined plateau at ca. –0.35 V can be still seen in the oxygen reduction voltammogram. This feature is less prominent and the current corresponding to it is lower (ca. –0.20 mA at –0.35 V) than those recorded at 50 mV/s (ca. –0.70 mA at –0.30 V). This can be due to the characteristics of planar semi-infinite diffusion through the microporous metal layers, which predict a peak-shaped voltammogram and higher currents at high scan rates and an S-shaped voltammogram and lower currents, as a diffusional steady state is approached. (Note that the ratio of currents is 0.70/0.2=3.5, comparable to the square root of the ratio of the corresponding scan rates which is $(50/5)^{1/2}=10^{1/2}=3.3$). It can also be seen that the oxygen reduction voltammograms are shifted in the sandwich-type sensor positive with respect to those obtained at the all-planar sensors of the previous sections.

This, again, is expected for a highly irreversible reaction like oxygen reduction: as the mass transfer rate increases, in the absence of a significant mass transfer barrier at Au all-planar devices, the kinetic control potential range is extended and the voltammogram is shifted to more negative potentials.

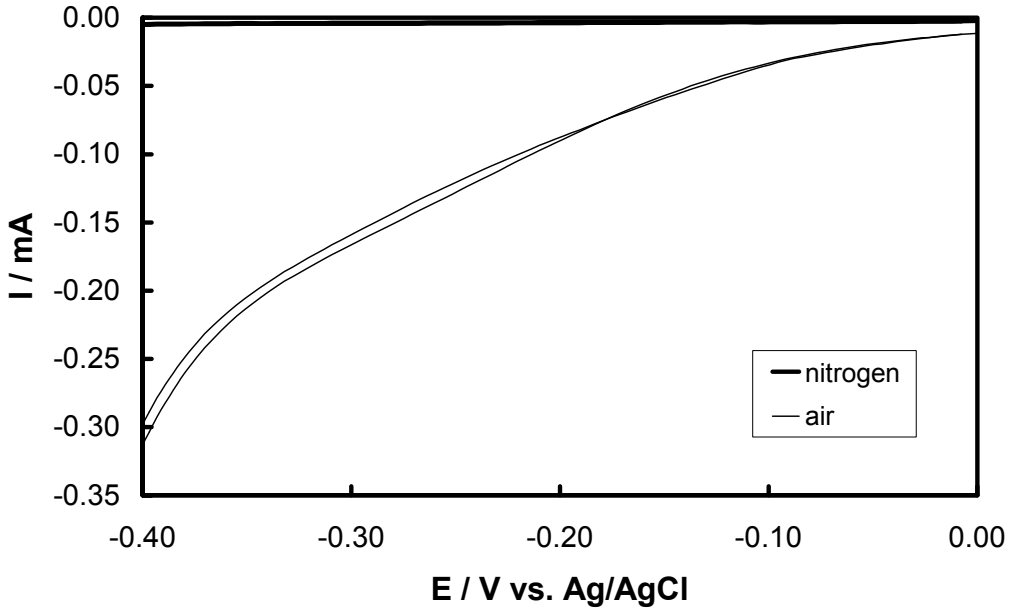

Fig. 10: *Voltammograms recorded at 5 mV/s in 60% RH nitrogen (thick line curve) and air (thin line curve) streams at a three-electrode Au (vs. Ag/AgCl)/Nafion®/Au STS sandwich device with a gold layer thickness of 1500 nm.*

Finally, the fact that the observed oxygen reduction currents for the sandwich-type sensor are of similar magnitude (if not higher) than those at the open all-planar sensor, is probably due to the fact that the mass transfer limitations introduced in the former case are offset by the increase in electroactive surface area since the sandwich electrode arrangement ensures a more uniform current distribution and a complete utilisation of the entire electrode layer (see also below). It has therefore been confirmed that with sandwich-type sensors the gas has to diffuse through the electrode layer to the electrode/electrolyte interface.

Sandwich Type Sensors (STS): Humidity Effects.

The sandwich-type devices were tested in the entire 20-100% RH range. Fig. 11(A) below shows their voltammetry in air streams of varied humidity at a scan rate of 50 mV/s, whereas Fig. 11(B) and its inset their voltammetry at 5 mV/s.

(**A** ... above; **B** ... below)

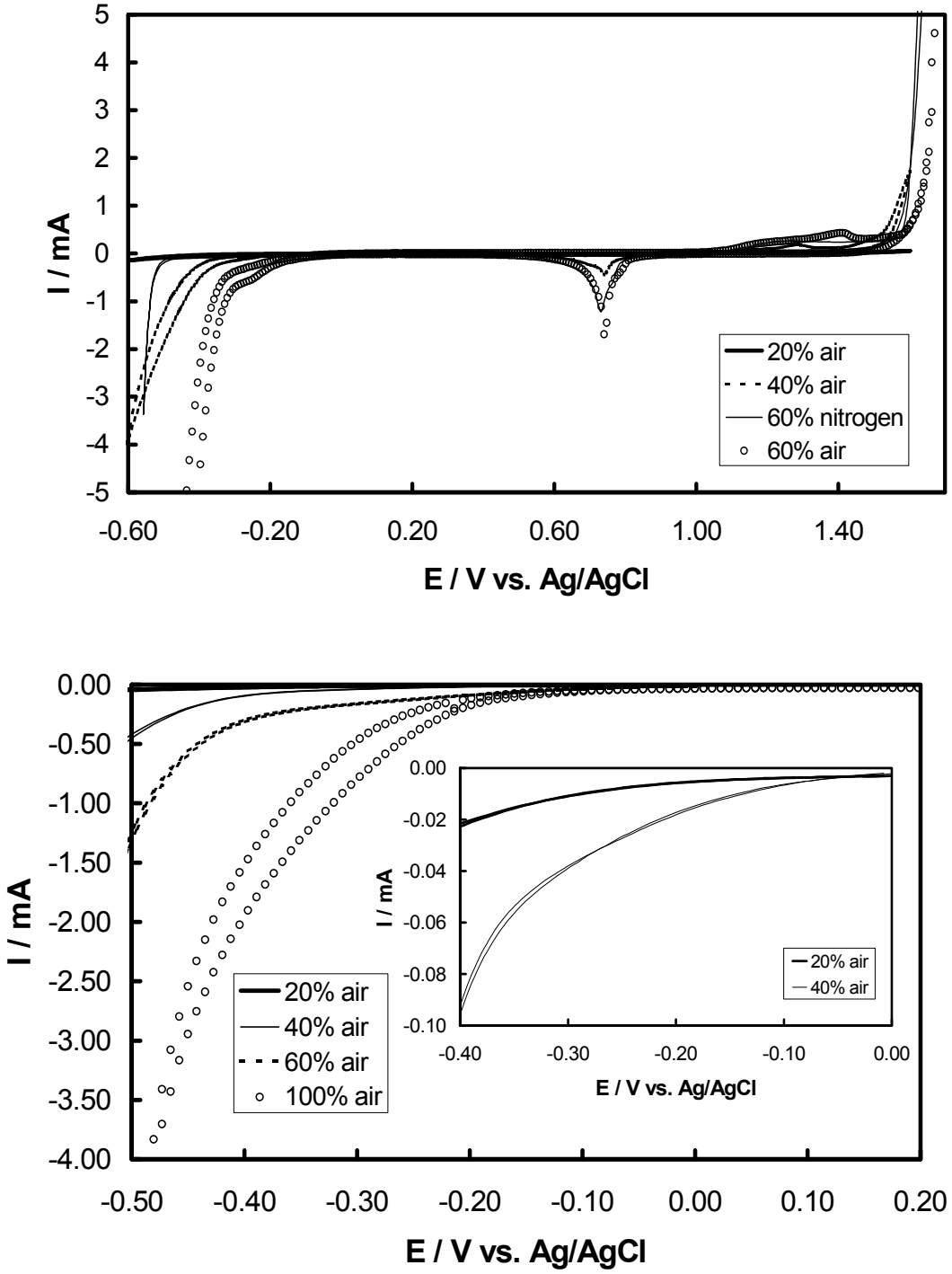

Fig. 11: *Voltammograms recorded at 50 mV.s^{-1} in water saturated nitrogen and air streams of varying humidity at three-electrode Au (vs. Ag/AgCl)/Nafion®/Au sandwich device with a gold layer thickness of 1500 nm* (**A**). *Voltammogram recorded at 5 mV/s in air streams of 20, 40, 60 and 100% RH at a three-electrode Au (vs. Ag/AgCl)/Nafion®/Au sandwich device. Inset same for air streams of 20 and 40% RH* (**B**).

It can be seen that the effect of humidity both on surface electrochemistry, in Fig. 11(A), as the oxide stripping peak and on oxygen reduction; as that in Fig. 11(B), is pronounced even in this type of sensor where the sandwich-type electrode arrangement ensures small ohmic losses through the thin (0.175 mm) and highly contacting Nafion® membrane (uncompensated resistance value measured at 20% RH was 320 Ω).

On a more quantitative basis, Table II below presents the charge (Q) corresponding to Au oxide stripping (indicative of electroactive surface area), the electroactive surface area (A_{el}), the current at –0.1 V ($I_{-0.1V}$) and the current at –0.1 V per electroactive surface area (true current density, $i_{-0.1V}$), both for the sandwich-type sensor (nominal WE area of 2.01 cm^2) and of an all-planar sensor (nominal WE area: 0.6 cm^2), for various humidity levels. For the sandwich-type sensor, the near-limiting current values (–0.3 to -0.4 V region) are also given.

Table II. *Au oxide reduction charge (Q), electroactive surface area (A_{el}), oxygen reduction current at –0.1 V ($I_{0.1V}$) and oxygen reduction current at –0.1 V per electroactive surface area (true current density,$i_{0.1V}$) for sandwich and planar type sensors (STS, PTS) for various humidity levels (RH%).*

Humidity / % RH	**Q** / μC		**A_{el}** / cm^2		**$I_{-0.1V}$** / μA		**$i_{-0.1V}$** / μA/cm^2	
	STS	PTS	STS	PTS	STS	PTS	STS	PTS
100	1800	319	4.3	0.8	60	50	14	62.5
60	1700	83.6	4	0.2	30	5	7.5	25
40	1200	39	2.9	0.1	10	1	3.5	10
20	450	5.8	1.1	0.015	1	0.1	0.9	6.7

Two points can be made on the results of Table 2. First, for both sensors the effect of humidity is more pronounced (especially at high RH values) on the oxygen reduction current ($I_{-0.1}$) than on the stripping charge-electroactive surface area (Q-A_{el}), indicating that the effect of water content on oxygen reduction is not merely a Au active site number effect but also due to the influence of water on reaction kinetics at the Au/Nafion® interface.

Second, the electroactive surface area of the sandwich-type STS device is generally higher than that of the planar PTS device (after correcting for the 2.01 cm^2 / 0.6 cm^2 ratio of their nominal working electrode area). This is another indication that, assuming a similar Au layer roughness factor and due to current distribution and ohmic loss considerations, in the planar arrangement some part of the working electrode layer lying far away from the counter electrode does not contribute to the observed current.

This fact, together with the presence of a much thicker mass transfer barrier in the case of the sandwich arrangement (resulting in partially mixed control at –0.1 V and signs of some current mass transfer limitations,) leads, in general, to the lower current densities measurable at the sandwich sensor.

Sandwich Type Sensors (STS): Oxygen Concentration Steps

The response of the sandwich-type sensor to oxygen concentration steps is shown in the current (at -0.25 V) vs. time curves presented for 100%RH and 40% RH gas streams in Figs. 12(A) and 12(B), respectively; both being illustrated below (on the following page). The insets in these Figures then depicts the respective "current vs. oxygen" calibration plots for the corresponding concentration range. As seen, reasonable linearity and detection limits less than 1 % (v/v) could be obtained.

Capillary Planar Type Sensors (CPTS): Voltammetry

The most common way to introduce a diffusion barrier is to use a capillary with dimensions greater than the mean free path of the gas molecules. In our capillary configuration experiments, the samples were humidified first prior to the introduction of a sensor lid bearing the capillary (1.5 mm) on top of the planar sensor device, to ensure even and accurate humidification of the Nafion® membrane.

The sensor was then tested in two different arrangements -- with both the lid on and off. Fig. 13(A) shows slow potential scan (5 mV/s) voltammograms at a capillary-type Au sensor in air and nitrogen gas streams of 100% RH. For comparison, Fig. 13(B) shows similar results obtained when the lid / capillary were removed, *i.e.,* when the same sensor was operated in an open-type mode.

(**A** ... above; **B** ... below)

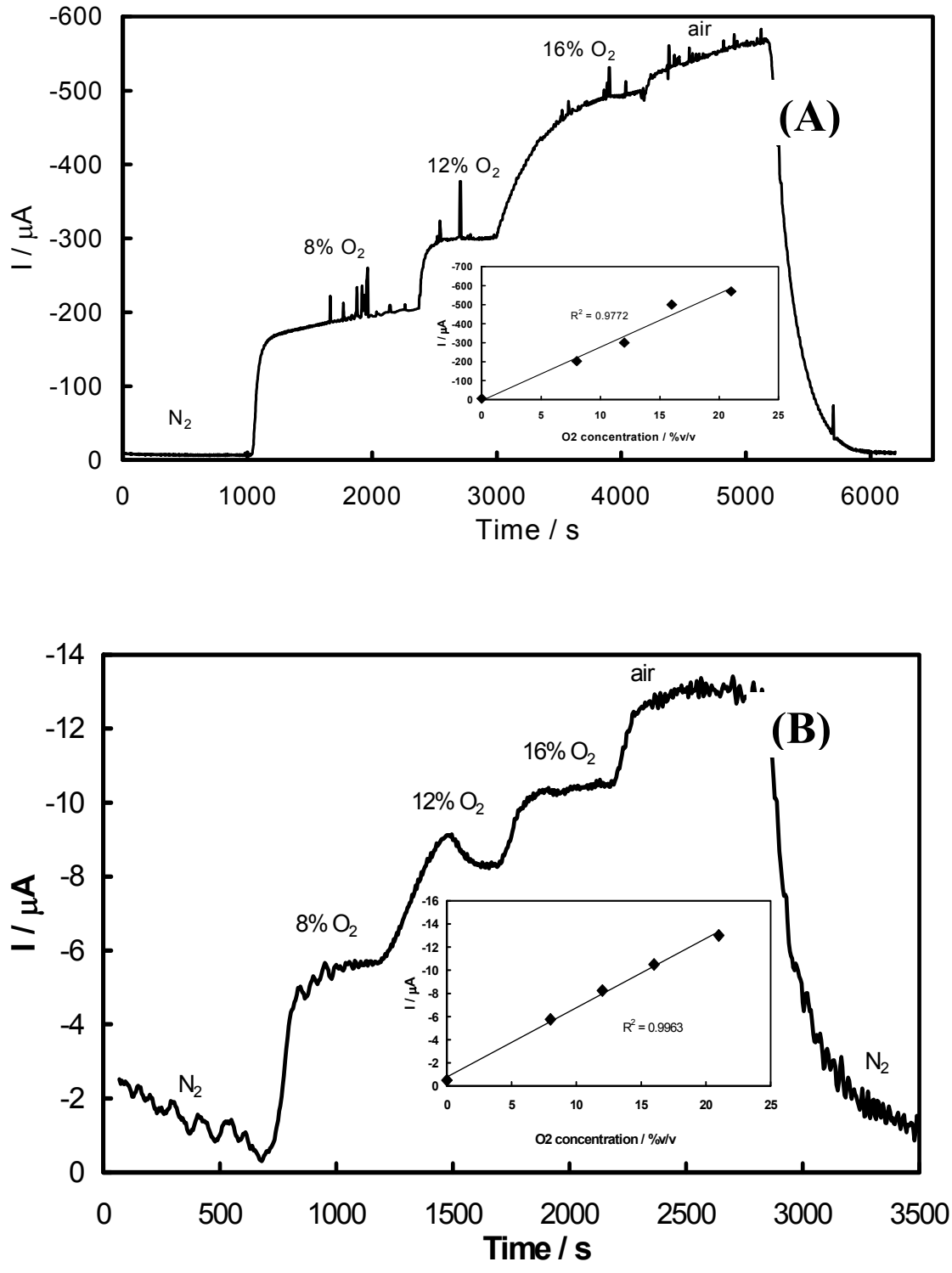

Fig. 12: *The "Current-to-time" response of the Au (vs. Ag/AgCl)/Nafion®/Au sandwich sensor to oxygen concentration steps at 100%* (**A**) *and 40% RH gas samples* (**B**). *The working electrode was held at –0.25 V vs. Ag/AgCl. Insets: Variation of the background-corrected current with oxygen concentration.*

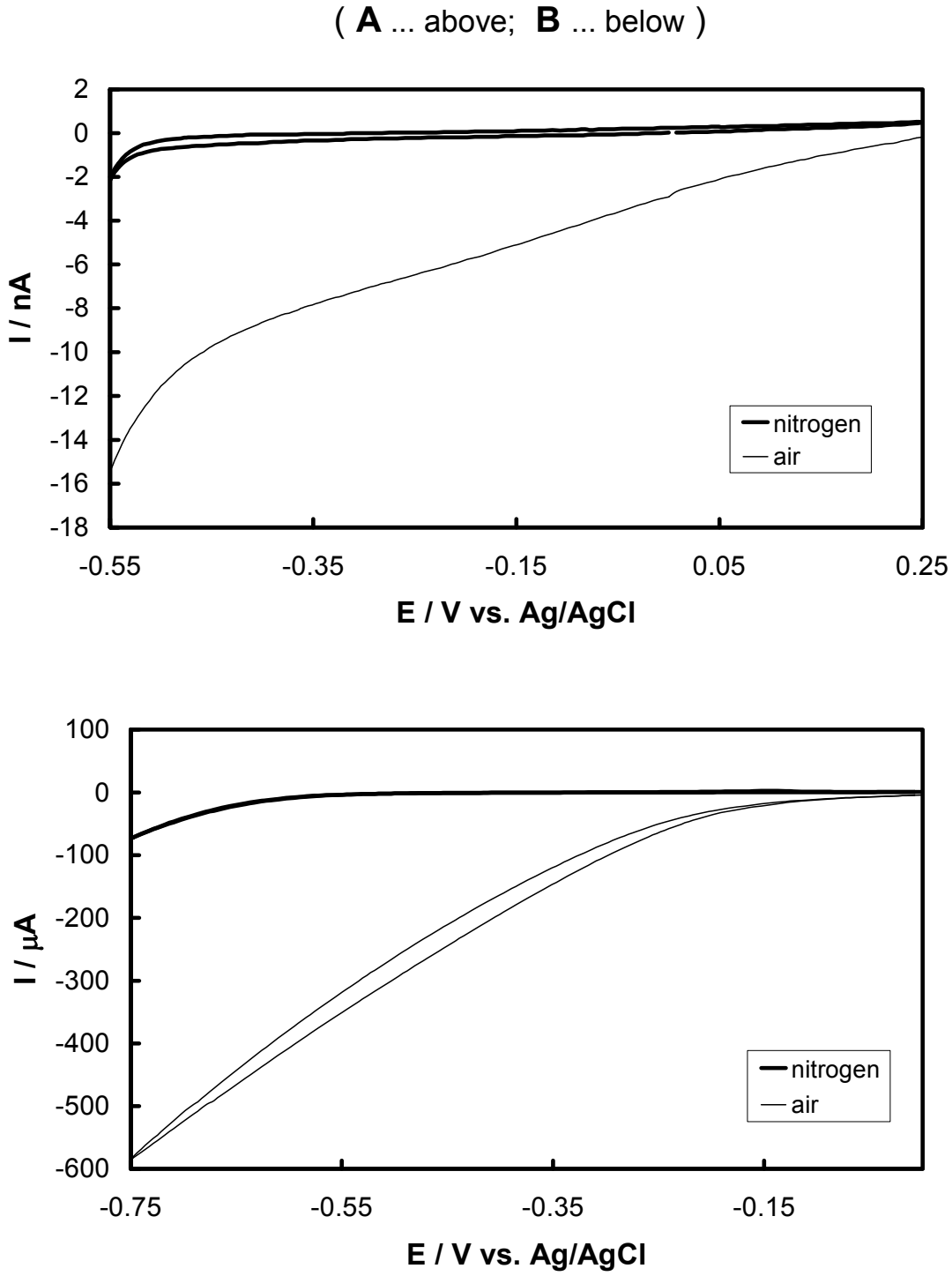

Fig. 13: *Slow scan voltammograms (at a 5 mV/s potential scan rate) for the capillary* (**A**) *and open-type* (**B**) *arrangements in air and nitrogen gas streams of 100% RH.*

One can clearly notice signs of an S-shaped voltammogram with an ill-defined plateau, as well as a dramatic decrease in current, in the case of the capillary arrangement. Both these findings are due to the introduction of a significant mass transfer barrier, that of the capillary.

Capillary Planar Type Sensors (CPTS): Humidity Effects

The effect of humidity on the near-limiting oxygen reduction current recorded at CPTS devices is shown in the following Table III:.

.

Humidity / %RH	**Limiting current** / nA
100	10
40	2.9
20	0.5

Table III. *Limiting currents and Tafel slopes measured by capillary sensor for various humidity levels*

It can be seen that, as in all other sensor configurations too, the oxygen reduction current decreases with decreasing humidity. The decrease of the limiting current can only be attributed to a decrease in the geometric electrode area due to a decrease in active-hydrated Au/Nafion® sites (and not to a change in the real electroactive surface area and oxygen reduction kinetics as in the case of kinetically controlled currents).

Capillary Planar Type Sensors (CPTS): Oxygen Concentration Steps

Finally, Fig. 14 shows the variation of current with time during oxygen concentration steps at a capillary-type sensor with the Au-WE held at –0.05 V vs. a Ag/AgCl strip ref. electrode.

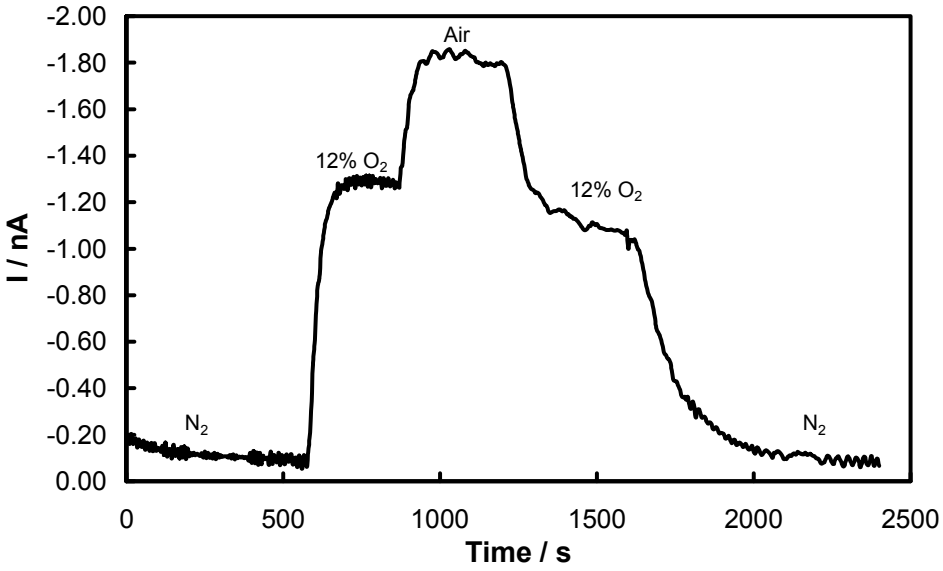

Fig. 14: *Current-time response of the Au (vs. Ag/AgCl)/Nafion®/Au capillary sensor to oxygen concentration steps at 100% RH gas samples. Note: The WE held at –0.05 V vs.Ag/AgCl.*

The estimated response time of the capillary sensor, T_{90} = 55 s, is equivalent of that measured with the simple PTS device (65 s, see Fig. 7). The rather high response times obtained with both arrangements should be due to the dead volumes of our gas tubing, humidification vessel and test cell since the T_{90} of a commercial fuel-cell type CiTiceL® sensor (City Technology Ltd) placed in the test cell simultaneously with the planar device was also 60 s (again, Fig. 7; specification of the sensor, with minimized dead volumes, reports $T_{95} \leq 10$ s). For the sandwich sensor the response time nearly doubled to 125 s (Fig. 12), in accordance with its comparatively thick diffusion barrier consisting of a porous metal layer.

Conclusions

Based on the previous presentation of the results and observations obtained, it can be stated:

(**i**) Planar and sandwich-type all-solid amperometric oxygen sensors were prepared by a simple metal sputtering technique on Nafion® solid polymer electrolyte membranes.

(**ii**) In the absence of a well-defined mass transfer barrier (planar type sensors, PTS) the current has been always under kinetic or mixed control while upon the introduction of a cappilary barrier (in cappilary planar type sensors, CPTS), as well as at sandwich type sensors (STS), signs of a limiting current appear.

(**iii**) The oxygen reduction signal at the polymer electrolyte sensors tested depended strongly on humidity, mainly due to a variation in active metal/electrolyte sites and oxygen reduction kinetics rather than to resistivity effects. For practical applications this dependence implies the need for a water reservoir that would keep the Nafion® membrane fully hydrated.

(**iv**) The sensors, based on thin layers of Au electrodes and Nafion®, performed comparably well (especially the planar-type devices) with a commercial fuel-cell type sensor (CiTiceL® sensor, City Technology Ltd), based on a high surface area Pt powder electrode and a liquid electrolyte. Their advantages include the use of a non-labour-intensive preparation technique and of cheaper catalytic electrodes (thin, continuous layers of Au).

Acknowledgements

European Union

This research has been co-financed by the European Union (European Social Fund – ESF) and Greek national funds through the Operational Program "Education and Lifelong Learning" of the National Strategic Reference Framework (NSRF) - Research Funding Program: Heracleitus II. Investing in knowledge society through the European Social Fund. Financial support from City Technology Ltd, UK and the Aristotle University of Thessaloniki, Basic Research Fund is also acknowledged

References

1. I. Bergman: *British Patent 1200595* (1970).
2. J. Evans, D. Pletcher, P.G. Warburton, T.K. Gibbs: *Anal.Chem.* ***61****(6)* (1989) 577.
3. B.S. Hobbs, A.D.S. Tantram, R. Chan-Henry, in: *Techniques and Mechanisms in Gas Sensing* (P.T. Moseley, J.O.W. Norris, D.E. Williams; Eds.), Adam Hilger, Bristol, 1991.
4. G. Schiavon, G. Zotti, G. Bontempelli: *Anal.Chim.Acta* ***221*** (1989) 27.
5. G. Schiavon, G. Zotti, G. Bontempelli, G. Farnia, G. Sandona: *Anal.Chem.* ***62****(3)* (1990) 293.
6. F. Opekar: *Electroanalysis* ***4*** (1992) 133.
7. P. Millet, A. Michas, R. Durand: *J.Appl.Electrochem.* ***26****(9)* (1996) 933.
8. N. Miura, H. Kato, Y. Ozawa, N. Yamazoe, T. Seiyama: *Chem.Lett.* ***11*** (1984) 1905.
9. V.P. Chviruk, O.V. Linyucheva, A.I. Buket: *Electrochim.Acta* ***42****(20-22)* (1997) 3155.
10. G. Alberti, R. Palomari: *Solid State Ionics* ***35*** (1989) 153.
11. G. Alberti, F. Cherubini, R. Palomari: *Sensors and Actuators B* ***24-25*** (1995) 270.
12. A.W.E. Hodgson, D. Pletcher, S. Sotiropoulos: *Sensors and Actuators B* ***50*** (1998) 181.
13. K. Wallgren, S. Sotiropoulos: *Anal.Chim. Acta* ***388*** (1999) 51.
14. K. Wallgren, S. Sotiropoulos: *Sensors and Actuators B* **60** (1999) 174.
15. M. Willet, in: *Proceedings of the 10th Conference on Sensors and their Applications* (N.M. White, A.T. Augousti; Eds.), Institute of Physics Publishing, Bristol, 1999.
16. *International Critical Tables* (1926-1930), National Research Counsil, US.
17. A. Capon, R. Parsons: *J.Electroanal.Chem.* ***39****(2)* (1972) 577.
18. H. Kita, H. Nakajima: *Electrochim. Acta* ***31****(2)* (1986) 193.
19. R. Amadelli, A. De Battisti, O. Enea: *J. Electroanal.Chem.* ***339*** (1992) 85.
20. M.S. El-Deab, T. Osaka: *Electrochem.Commun.* ***4*** (2002) 288.
21. T.A. Zawodzinski, T.E. Springer, J. Davey, J. Valerio, S.Gottesfeld, in Modelling *of Batteries and Fuel Cells* (R.E. White, M.W. Verbrugge, J.F. Stockel; Eds.), Vol. 91-10, p.187, The Electrochemical Society Proceedings Series, NJ, 1991.
22. Y. Sone, D. Ekolunge, D. Simonsson: *J. Electrochem. Soc.****143****(4)* (1996) 1254.
23. J.J. Sumner, S.E. Creager, J.J. Ma, D.D Des Maiteau: *J.Electrochem. Soc.* ***145*** *(4)* (1998) 107.
24. S.K. Zecevic, J.S. Wainright, M. Litt, S.Lj. Gojkovic, R.F.Savinell: *J. Electrochem. Soc.* ***144*** (1997) 2973.
25. F. Uribe, T.E. Springer, S. Gottesfeld: *J. Electrochem. Soc.* ***139*** (1992) 567.